RSC Advances

PAPER

View Article Online
View Journal | View Issue

Cite this: *RSC Adv.*, 2022, **12**, 16046

Synthesis of pH-responsive covalent organic frameworks nanocarrier for plumbagin delivery

Yang Wang, *[ab] Xin Sun[a] and Yi Wang[b]

Received 17th May 2022
Accepted 21st May 2022

DOI: 10.1039/d2ra03127b

rsc.li/rsc-advances

Covalent organic frameworks have attracted increasing attention in the fields of nanotechnology and nanoscience. However, the biomedical applications of COFs still remain less explored. Here, a new type of nanoscale covalent organic framework (COF-366) composite was prepared by a facile solvothermal method. The obtained material was characterized by powder X-ray diffraction (XRD), Fourier transform-infrared spectroscopy (FTIR), and scanning electron microscopy (SEM). The results showed that the COF-366 nanocarriers possess uniform spherical morphology with a diameter of 150 nm, which make them favourable for drug delivery. After the plumbagin encapsulation, an effective pH responsive release, high adsorption capacity, and good biocompatibility were achieved. These characteristics make nanoscale COF-366 an ideal material for drug delivery and reveal its promising application in biomedical applications.

1 Introduction

As a natural naphthoquinone constituent, plumbagin (PLB) has been found to possess anticancer effects.[1,2] Earlier studies have demonstrated that the anticancer effects of PLB are mainly due to apoptosis and autophagy, cell cycle arrest, and induction of intracellular reactive oxygen species generation.[3–5] However, the drawbacks related to a short half-life range, from 36 min to 5 h, and poor water solubility of PLB restrict its clinical translational application and therapeutic effects.[6] In this respect, a sustained PLB delivery system which can improve the delivery efficiency and loading capacity obviously becomes the major trend.

In recent years, many efforts on drug delivery have been made to ensure efficient therapy.[7–9] It is noteworthy that several materials, such as nanoemulsions, glycerosome gels, and metal organic frameworks have been developed for PLB delivery.[10–13] However, many of the host materials have inherent limitations (low surface area, low drug loading capacity) to becoming a successful drug delivery system. Thus, it is imperative to seek novel materials with impressive properties to improve the drug delivery performance.

As an emerging material of self-assembled porous structure, covalent organic framework (COF) is conjugate crystalline polymer.[14–17] Due to the versatility of COF, such as large specific surface area, controllable pores and structure as well as high porosity, COF has demonstrated great potential for separation, heterogeneous catalysis, and sensing.[18–20] However, much attention has been less paid to the establishment of COF based drug carriers for the intended applications. For example, Zhao *et al.* designed two porous COF as drug nanocarriers. After an anticancer drug (5-FU) was encapsulated, the materials demonstrated high loading capacity and sustained release behavior.[21] A very recent study by Li *et al.* have reported the synthesized of a porous Cage-COF-TT, which exhibits highly thermal stability and loading capacity. The composite was employed to effectively deliver three representative drugs.[22] Tsai *et al.* have also designed a thioether-terminated triazole bridge-containing COF (TCOF). The TCOF was sensitive to pH and processed biocompatibility toward HeLa cells.[23] All these studies demonstrated that COF as novel are potential in drug delivery for therapeutic applications.

Herein, COF-366 nanocomposite with a uniform size was synthesized and successfully used as a host material for the PLB encapsulation (denoted as PLB@COF-366) and delivery. The results indicated that PLB@COF-366 nanocomposite is a physiological pH responsive drug delivery system, and PLB release from PLB@COF-366 is faster in mild acidic conditions (pH = 5.5) than under physiological acidity (pH = 7.4). The loading capacity was calculated to be 16.3 wt%. The high biocompatibility of COF-366 nanocomposite was further demonstrated by *in vitro* MTT assay toward pancreatic cancer cells.

2 Experimental

2.1 Materials

Plumbagin, tetra-(amidogen phenyl)-porphine (TAPP) and terephthaldehyde (BDA) were booked from Aladdin. Chemicals such as methanol purchased from Sinopharm Chemical Reagent. Phosphate buffer solution was prepared by using

[a]*Engineering Research Center of Clinical Functional Materials and Diagnosis & Treatment Devices of Zhejiang Province, Wenzhou Institute, University of Chinese Academy of Sciences, Wenzhou 325024, China. E-mail: wangyzu@126.com*
[b]*School of Chemistry and Chemical Engineering, Yangzhou University, Yangzhou 225002, China*

0.1 mol L^{-1} NaH_2PO_4/Na_2HPO_4 stock solution. All other chemicals were of analytical regent grade. And the double deionized water was prepared using a Millipore water purification system (resistance > 18 MΩ cm^{-1}, Bedford, MA, USA).

2.2 Apparatus

Scanning electron microscopy (SEM, Hitachi S-4800, 15 kV, Japan) was utilized to analyze the surface morphology of the products. Powder X-ray diffraction (PXRD) was performed by D8 Advanced X-ray diffractometer (Bruker Co., Germany) in the range of 5 to 80°. The Fourier transform infrared spectroscopy (FTIR) was measured *via* Bruker tensor 27 infrared microscopic spectrometer (Bruker Co., Germany). UV-vis absorption was detected with a Hitachi U-3010 spectrophotometer.

2.3 Synthesize of COF-366 and PLB@COF-366

The main paragraph text follows directly on here. COF-366 was synthesized based on the previous reports with some modifications.[24] Tetra(*p*-amino-phenyl)porphyrin (TAPP) (27.0 mg, 0.04 mmol), terephthaldehyde (11.2 mg, 0.08 mmol), 1.0 mL of absolute EtOH, 1.0 mL of mesitylene and 0.2 mL of 6 mol L^{-1} aqueous acetic acid were mixed together and stirred at room temperature for 15 min. Then the mixture was heated to 120 °C for three days in a 25 mL teflon-lined stainless steel container. After the mixture was cooled, purple solid was separated, then washed with 1,4-dioxane, THF, and acetone, and dried at 40 °C under vacuum for 12 h to obtain a purple powder. For the synthesis of PLB@COF-366 (Fig. 1), the obtained crystal powder (33.3, 50 and 66.6 mg) was placed into the 10 mL ethanol solution of PLB (10 mg) and then stirred under room temperature condition for 9 h. PLB@COF-366 was obtained by filtrating and washing the product with methanol for three times to take out the excess drugs in the solvent and drying it in a vacuum stove. Subsequently, 0.1 g PLB@COF-366 was dispersed in 20 mL H_2O with the addition of 0.3 g PVP. The mixture kept stirring for 12 h. After that, resultant nanocomposite was washed with water for about five times and then dried in vacuum stove before use. In addition, different amounts of COF-366 (50, and 66.6 mg) were also used to fabricate PLB@COF-366 for comparison of their drug loading capacity. The drug loading capacity and drug encapsulation efficiency were calculated by the following equations:

$$\text{Drug loading capacity} = \frac{\text{weight of the loaded drug}}{\text{weight of COF-366}} \times 100\%$$

$$\text{Drug encapsulation efficiency} = \frac{\text{weight of the loaded drug}}{\text{weight of initial total drug}} \times 100\%$$

3 Results and discussion

The obtained materials were characterized by powder X-ray diffraction to confirm the successful formation of COF-366 and PLB@COF-366 nanocomposites. As displayed in Fig. 2A, the main diffraction peaks of both materials at 3.5°, 5.12°, 6.3° and 8.0° were corresponded to the (100), (110), (200), and (210) planes, respectively, which is consistent with the previous literature.[25,26] The results also indicated that COF-366 still maintains its high crystallinity after the encapsulation of PLB. The Fourier-transform infrared spectroscopy (FTIR) spectrum was measured to verify the chemical structures of PLB and PLB@COF-366. As shown in Fig. 2B, the characteristic peak at 3343 cm^{-1} was ascribed to the amide –OH stretching of PLB.[27] As for COF-366, a characteristic peak at about 1623 cm^{-1} corresponded to the stretching C=N bonds from the linkage of organic ligand. Two characteristic peaks at 1691 cm^{-1} and 3360 cm^{-1} can be allocated to the residual aldehyde group and amino, respectively.[28,29] In comparison to the spectrum of PLB and COF-366, the main characteristic peaks of PLB@COF-366 match well with the curves of PLB and COF-366, suggesting the encapsulation of PLB would not change the crystallinity of COF-366. This is consistent with the above results of XRD.

The size and morphology of COF-366 and PLB@COF-366 were investigated by SEM. It can be observed that the monodispersed nanocrystals with a mean diameter of *ca.* 150 nm are mainly spherical in shape (Fig. 3A). This size matches well with

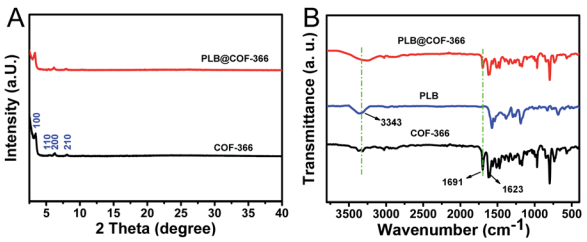

Fig. 2 (A) XRD patterns and (B) FTIR spectra of COF-366 and PLB@COF-366.

Fig. 1 Schematic illustration of the preparation process of nanoscale COF-366 and PLB@COF-366.

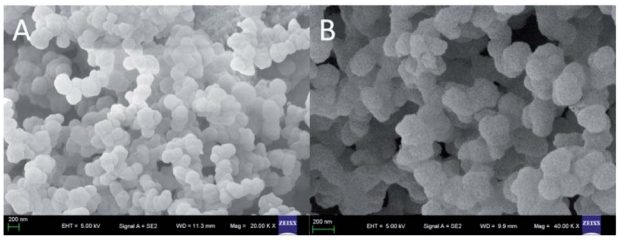

Fig. 3 SEM images of (A) COF-366 and (B) PLB@COF-366 nanocomposite.

the reported suitable nanoparticle diameter for the effective cell uptake. Hence, it is anticipated that the obtained COF-366 could be internalized into cells effectively. After the encapsulation of PLB, the geometrical structure of COF-366 was retained but its surface became a litter rough (Fig. 3B). This finding suggests that the successful formation of PLB@COF-366 nanocomposite.

Thermogravimetric analysis was carried out to investigate the thermal stability of COF-366. As shown in Fig. 4, a slight weight loss of 17.42% occurred at low temperatures, which was attributed to the removal of adsorbed molecules such as H_2O and small organic precursors. Subsequently, the dramatic decomposition between 400 and 800 °C with a weight retention of 50.17% was due to the decomposition of the COF-366, demonstrating its excellent thermal stability. The specific surface area was determined using nitrogen adsorption isotherms at 77 K, and the Brunauer–Emmett–Teller (BET) surface area was found to be 1240 $m^2\ g^{-1}$, which was beneficial for drug loading and delivery applications. A substantial decrease in the BET area (560 $m^2\ g^{-1}$) occurred after the incorporation of PLB, indicating PLB was successfully immobilized into the internal pores of COF-366.

In order to investigate the encapsulating and controlled release behavior of the prepared COF-366 nanocomposite, PLB was selected as a model anti-cancer drug. As shown in Fig. 5, an obvious UV-vis absorption spectrum of PLB was observed at 480 nm, and the absorbance intensity is proportional to the PLB concentration in a wider range of 5 to 50 mg L^{-1}. The linear regression equation was calculated to be $A = 0.023C$ (mg L^{-1}) + 0.0251 ($R^2 = 0.9971$). COF-366 was immersed in an aqueous PLB solution under agnetically stirred overnight for drug encapsulation. The resultant nanocomposite was collected by filtration, and washed with water. UV-vis absorption spectra were used to determine the content of the original PLB solution and the residual PLB in the supernatant after interaction with COF-366. The drug loading capacity decreased in a sequence of PLB@COF-366 (16.3 wt%) > PLB@COF-366-2 (10.8 wt%) > PLB@COF-366-3 (8.2 wt%) with the change of COF-366 contents (33.3, 50, and 66.3 mg), suggesting that COF-366 (33.3 mg) was favorable for the drug loading. In addition, the drug encapsulation efficiency was calculated to be 54.3%. The high loading capacity of COF-366 for the encapsulation of PLB could occur for two reasons: (I) COF-366 is synthesized by organic linkers. So it is possible to interact with the PLB organic molecules through π–π stacking interaction;[30] (II) the relative high surface area of COF-366 could improve the adsorption capacity of PLB.

An efficient pH-responsive delivery system should be characterized by the slow and sustained release property. This is great for preventing the drug dissipation before it reaches the cancer cells. Compared to normal tissues at physiological pH, the extracellular microenvironments of tumors are mildly acidic. Hence, dialysis bag with PLB encapsulated COF-366 were immersed in PBS solution and investigated at different pH values of 5.5 and 7.4 at room temperature. After selected time intervals, the amount of PLB releasing from PLB@COF-366 was determined. As shown in Fig. 6, PLB encapsulated PLB@COF-366 nanocomposite demonstrated sustained release without any burst dissociation. Around of 93% of encapsulated PLB was released into the 5.5 pH solution after 72 hours. In comparison, PLB@COF-366 nanocomposite exhibited a slower release profile at a pH value of 7.4 within the same period. The pH-sensitive released PLB continuously increased due to the acid-promoted dissolution of COF-366. Hence PLB@COF-366 nanocomposite with a pH responsive drug release property are promising as drug carriers for targeted drug release to the different pH values between acidic tumour sites and normal tissues. In addition, the BET surface area of COF-366 was reduced to 420 $m^2\ g^{-1}$ after the release of PLB, probably due to the structure of COF-366 was partially destroyed under acidic conditions. The release kinetic and mechanism of PLB@COF-366 was analyzed using Baker–Lonsdale, Higuchi, zero order, and first order kinetic models. The regression coefficient (R^2)

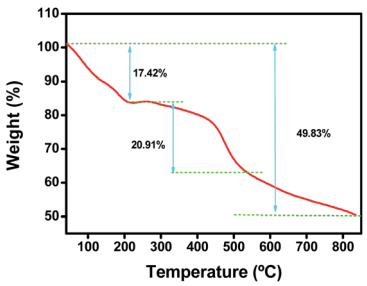

Fig. 4 Thermogravimetric analysis curve of COF-366.

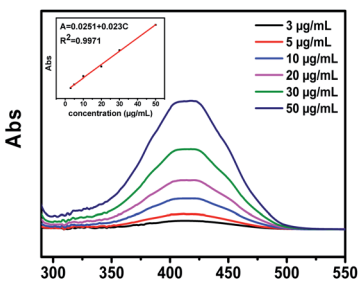

Fig. 5 UV-vis absorption spectrum of PLB in the pH 5.5 solution. The inset shows the relationship between absorbance intensity and PLB concentration.

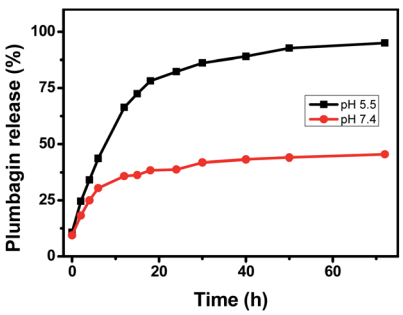

Fig. 6 PLB release profiles from COF-366 in simulated physiological solution with pH values of 5.5 and 7.4.

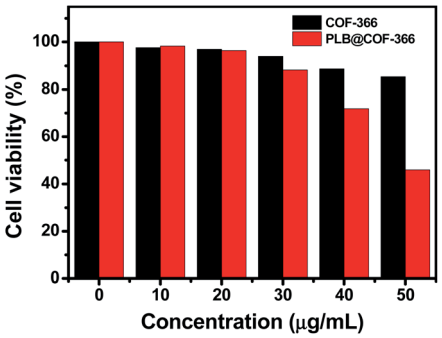

Fig. 7 Cell viability after exposure to COF-366 and PLB@COF-366.

values for each model were 0.9568, 0.9425, 0.9015, and 0.8627, respectively. Hence we can conclude that the Baker–Lonsdale model generates a more satisfactory fit to the experimental data with the highest R^2 values. The calculated kinetic exponent was 0.6257, suggesting that PLB release from COF-366 are non-Fickian transport mechanism.

Nontoxicity or low-toxicity is necessary for further bio-applications likewise. Hence, the cytotoxicity of the COF-366 nanocomposite against human prostate cell lines LNCap was examined using standard 3-(4,5-dimethyl-thiazol-2-yl)-2,5-diphenyltetrazolium bromide (MTT) assays. LNCap cells were incubated with the COF-366, and PLB@COF-366 nanocomposite at different concentrations for 24 h. As shown in Fig. 7, the COF-366 nanocomposite exhibited excellent biocompatibility. Negligible changes in cell viability after 24 h of incubation were found. Even when the concentration of COF-366 nanocomposite was over 40 μg mL^{-1}, the cell proliferation is slightly hindered. The relatively good biocompatibility of COF-366 nanocomposite shows their potential use as an excellent nanocarrier *in vitro*. After LNCap cells were treated with PLB@COF-366 for 24 h, PLB@COF-366 nanocomposite exhibited higher inhibition to the growth of LNCap cells due to the encapsulating of PLB. But the cells could keep a high viability of 85% at the maximum dosage of 30 μg mL^{-1}. The results suggested that PLB@COF-366 nanocomposite is a high biocompatibility drug carrier material.

4 Conclusions

In summary, a nanoscale COF-366 nanocomposite was synthesized by a facile method. Considering its structural characteristics, COF-366 nanocomposite was employed as a host for the encapsulation and delivery of the anticancer drug PLB, and the release of targeted drug demonstrated pH-dependent behavior and a sustained release pattern over three days. Moreover, the carriers demonstrated a large drug loading capacity and lower cytotoxicity against the human prostate cell lines (LNCap). In addition, a postsynthetic strategy could be adopted to prepare other functional nanomaterials for the development of highly pH-sensitive and targeted nanocarrier. It is clear that, given the promising results obtained for covalent organic framework based PLB pharmaceutical delivery, further studies will focus on a broader range of COF-366 and PLB combinations to suppress gastric cancer or lung injury therapy. The related studies in our laboratory are in progress.

Conflicts of interest

There are no conflicts to declare.

Acknowledgements

This work was financially supported by Engineering Research Center of Clinical Functional Materials and Diagnosis & Treatment Devices of Zhejiang Province (WIUCASK20007).

Notes and references

1 I. Sharma, D. Gussain and V. P. Dixit, Hypolipidaemic and antiatherosclerotic effects of plumbagin in rabbits, *Indian J. Physiol. Pharmacol.*, 1991, **35**, 10–14.
2 A. A. Powolny and S. V. Singh, Plumbagin-induced apoptosis in human prostate cancer cells is associated with modulation of cellular redox status and generation of reactive oxygen species, *Pharm. Res.*, 2008, **25**, 2171–2180.
3 R. Gomathinayagam, S. Sowmyalakshmi, F. Mardhatillah, R. Kumar, M. A. Akbarsha and C. Damodaran, Anticancer mechanism of plumbagin, a natural compound, on non-small cell lung cancer cells, *Anticancer Res.*, 2008, **28**, 785–792.
4 J. Sun and R. J. McKallip, Plumbagin treatment leads to apoptosis in human K562 leukemia cells through increased ROS and elevated TRAIL receptor expression, *Leuk. Res.*, 2011, **35**, 1402–1408.
5 V. R. Sunil, K. N. Vayas, E. V. Abramova, R. Rancourt, J. A. Cervelli, R. Malaviya, M. Goedken, A. Venosa, A. J. Gow, J. D. Laskin and D. L. Laskin, Lung injury, oxidative stress and fibrosis in mice following exposure to nitrogen mustard, *Toxicol. Appl. Pharmacol.*, 2020, **387**, 114798.
6 W. Sumsakul, T. Plengsuriyakarn and K. Na-Bangchang, Pharmacokinetics, toxicity, and cytochrome P450 modulatory activity of plumbagin, *BMC Pharmacol. Toxicol.*, 2016, **17**, 50.
7 N. Mokhtari, S. Taymouri, M. Mirian and M. Dinari, Covalent triazine-based polyimine framework as a biocompatible pH-dependent sustained-release nanocarrier for sorafenib: An in vitro approach, *J. Mol. Liq.*, 2020, **297**, 111898.
8 M. Dinari, N. Mokhtari, S. Taymouri, M. Arshadi and A. Abbaspourrad, Covalent polybenzimidazole-based triazine frameworks: A robust carrier for non-steroidal anti-inflammatory drugs, *Mater. Sci. Eng., C*, 2020, **108**, 110482.
9 X. H. Zheng, L. Wang, Q. Pei, S. S. He, S. Liu and Z. G. Xie, Metal-organic framework@porous organic polymer nanocomposite for photodynamic therapy, *Chem. Mater.*, 2017, **29**, 2374–2381.
10 A. Chrastina, V. T. Baron, P. Abedinpour, G. Rondeau, J. Welsh and P. Borgstrom, Plumbagin-loaded nanoemulsion drug delivery formulation and evaluation of

antiproliferative effect on prostate cancer Cells, *BioMed Res. Int.*, 2018, **2018**, 9035452.

11 S. Md, N. A. Alhakamy, H. M. Aldawsari, M. Husain, N. Khan, M. A. Alfaleh, H. Z. Asfour, Y. Riadi, A. L. Bilgrami and M. H. Akhter, Plumbagin-loaded glycerosome gel as topical delivery system for skin cancer therapy, *Polymers*, 2021, **13**, 923.

12 Q. Li, H. Luo, Y. Y. Luo, W. Zhang, H. M. Hong, M. S. Deng, Y. Wang, B. Xu, G. B. Song and C. X. Xu, Plumbagin-loaded ZIF-90 nanoparticles suppress gastric cancer progression by targeting the YAP1 signaling, *Chem. Eng. J.*, 2022, **437**, 135369.

13 Y. Wang, Q. Li, M. Deng, K. Chen and J. Wang, Self-assembled metal-organic frameworks nanocrystals synthesis and application for plumbagin drug delivery in acute lung injury therapy, *Chin. Chem. Lett.*, 2022, **33**, 324–327.

14 N. Mokhtari, M. M. Khataei, M. Dinari, B. H. Monjezi and Y. Yamini, Imine-based covalent triazine framework: Synthesis, characterization, and evaluation its adsorption, *Mater. Lett.*, 2020, **263**, 127221.

15 N. Mokhtari, M. Afshari and M. Dinari, Synthesis and characterization of a novel fluorene-based covalent triazine framework as a chemical adsorbent for highly efficient dye removal, *Polymer*, 2020, **195**, 122430.

16 N. Mokhtari, M. M. Khataei, M. Dinari, B. Hosseini Monjezi, Y. Yamini and M. Hatami, Solid-phase extraction and microextraction of chlorophenols and triazine herbicides with a novel hydrazone-based covalent triazine polymer as the adsorbent, *Microchem. J.*, 2021, **160**, 105634.

17 M. Afshari and M. Dinari, Synthesis of new imine-linked covalent organic framework as high efficient absorbent and monitoring the removal of direct fast scarlet 4BS textile dye based on mobile phone colorimetric platform, *J. Hazard. Mater.*, 2020, **375**, 121514.

18 Z. Wang, S. Zhang, Y. Chen, Z. Zhang and S. Ma, Covalent organic frameworks for separation applications, *Chem. Soc. Rev.*, 2020, **49**, 708–735.

19 Y. Yusran, H. Li, X. Guan, Q. Fang and S. Qiu, Covalent Organic Frameworks for Catalysis, *EnergyChem*, 2020, **2**, 100035.

20 X. Liu, D. Huang, C. Lai, G. Zeng, L. Qin, H. Wang, H. Yi, B. Li, S. Liu, M. Zhang, R. Deng, Y. Fu, L. Li, W. Xue and S. Chen, Recent advances in covalent organic frameworks (COFs) as a smart sensing material, *Chem. Soc. Rev.*, 2019, **48**, 5266–5302.

21 L. Bai, S. Z. F. Phua, W. Q. Lim, A. Jana, Z. Luo, H. P. Tham, L. Zhao, Q. Gao and Y. Zhao, Nanoscale covalent organic frameworks as smart carriers for drug delivery, *Chem. Commun.*, 2016, **52**, 4128–4131.

22 M. Li, Y. Peng, F. Yan, C. Li, Y. He, Y. Lou, D. Ma, Y. Li, Z. Shi and S. Feng, A cage-based covalent organic framework for drug delivery, *New J. Chem.*, 2021, **45**, 3343–3348.

23 R. Anbazhagan, R. Krishnamoorthi, S. Kumaresan and H. C. Tsai, Thioether-terminated triazole-bridged covalent organic framework for dual-sensitive drug delivery application, *Mater. Sci. Eng., C*, 2021, **120**, 111704.

24 J. Wang, X. Yang, T. Wei, J. Bao, Q. Zhu and Z. Dai, Fe-porphyrin-based covalent organic framework as a novel peroxidase mimic for a one-pot glucose colorimetric assay, *ACS Appl. Bio Mater.*, 2018, **1**, 382–388.

25 S. Wan, F. Gandara, A. Asano, H. Furukawa, A. Saeki, S. K. Dey, L. Liao, M. W. Ambrogio, Y. Y. Botros, X. F. Duan, S. Seki, J. F. Stoddart and O. M. Yaghi, Covalent organic frameworks with high charge carrier mobility, *Chem. Mater.*, 2011, **23**, 4094–4097.

26 K. Xu, Y. Dai, B. Ye and H. Wang, Two dimensional covalent organic framework materials for chemical fixation of carbon dioxide: excellent repeatability and high selectivity, *Dalton Trans.*, 2017, **46**, 10780–10785.

27 P. Zhu, S. Li, S. Zhou, N. Ren, S. Ge, Y. Zhang, Y. Wang and J. Yu, In situ grown COFs on 3D strutted graphene aerogel for electrochemical detection of NO released from living cells, *Chem. Eng. J.*, 2021, **420**, 127559.

28 N. Duraipandy, R. Lakra, S. Kunnavakkam Vinjimur, D. Samanta, P. S. Korrapati and M. S. Kiran, Caging of plumbagin on silver nanoparticles imparts selectivity and sensitivity to plumbagin for targeted cancer cell apoptosis, *Metallomics*, 2014, **6**, 2025–2033.

29 D. Wang, Z. Zhang, L. Lin, F. Liu, Y. Wang, Z. Guo, Y. Li, H. Tian and X. Chen, Porphyrin-based covalent organic framework nanoparticles for photoacoustic imaging-guided photodynamic and photothermal combination cancer therapy, *Biomaterials*, 2019, **223**, 119459.

30 Y. Chen, Y. Xie, X. Sun, Y. Wang and Y. Wang, Tunable construction of crystalline and shape-tailored Co_3O_4@TAPB-DMTP-COF composites for the enhancement of tert-butylhydroquinone electrocatalysis, *Sens. Actuators, B*, 2021, **331**, 129438.